BIOCHEMISTRY
including biophysical chemistry & molecular biology

Article

pubs.acs.org/biochemistry

Stable Closure of the Cytoplasmic Half-Channel Is Required for Efficient Proton Transport at Physiological Membrane Potentials in the Bacteriorhodopsin Catalytic Cycle

Ting Wang,[†,§] Christoph Oppawsky,[‡,§] Yong Duan,[†] Jörg Tittor,[‡] Dieter Oesterhelt,[‡] and Marc T. Facciotti*[,†]

[†]Department of Biomedical Engineering and Genome Center, 451 East Health Science Drive, University of California, Davis, California 95616-8816, United States

[‡]Max Planck Institut für Biochemie, Martinsried D-82152, Germany

Supporting Information

ABSTRACT: The bacteriorhodopsin (BR) Asp96Gly/Phe171Cys/Phe219Leu triple mutant has been shown to translocate protons 66% as efficiently as the wild-type protein. Light-dependent ATP synthesis in haloarchaeal cells expressing the triple mutant is 85% that of the wild-type BR expressing cells. Therefore, the functional activity of BR seems to be largely preserved in the triple mutant despite the observations that its ground-state structure resembles that of the wild-type M state (i.e., the so-called cytoplasmically open state) and that the mutant shows no significant structural changes during its photocycle, in sharp contrast to what occurs in the wild-type protein in which a large structural opening and closing occurs on the cytoplasmic side. To resolve the contradiction between the apparent functional robustness of the triple mutant and the presumed importance of the opening and closing that occurs in the wild-type protein, we conducted additional experiments to compare the behavior of wild-type and mutant proteins under different operational loads. Specifically, we characterized the ability of the two proteins to generate light-driven proton currents against a range of membrane potentials. The wild-type protein showed maximal conductance between −150 and −50 mV, whereas the mutant showed maximal conductance at membrane potentials >+50 mV. Molecular dynamics (MD) simulations of the triple mutant were also conducted to characterize structural changes in the protein and in solvent accessibility that might help to functionally contextualize the current−voltage data. These simulations revealed that the cytoplasmic half-channel of the triple mutant is constitutively open and dynamically exchanges water with the bulk. Collectively, the data and simulations help to explain why this mutant BR does not mediate photosynthetic growth of haloarchaeal cells, and they suggest that the structural closing observed in the wild-type protein likely plays a key role in minimizing substrate back flow in the face of electrochemical driving forces present at physiological membrane potentials.

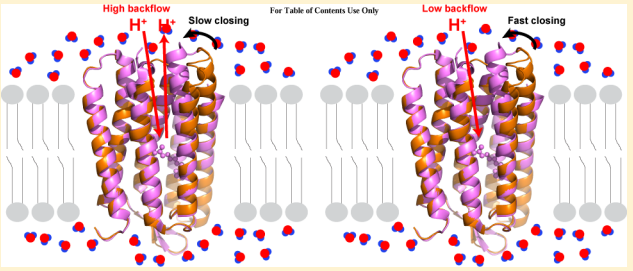

Bacteriorhodopsin (BR) is a retinal-containing protein of the halophilic Archaea.[1,2] Absorption of an actinic photon by BR initiates a catalytic cycle that drives the outward-directed translocation of a proton. The collective activity of numerous BRs thereby generates an electrochemical proton gradient that can be used to drive various cellular processes. The retinal chromophore is covalently bound, via a protonated Schiff base, to Lys216, which is located in the middle of the membrane. In addition to their role in light absorption, the retinal and the Schiff base also constitute a central component of the proton translocation pathway, dividing it into cytoplasmic and extracellular halves. The catalytic cycle is composed of a linear sequence of spectroscopically distinct intermediates called J, K, L, M, N, and O, with each described by a characteristic absorption maxima.[3−7] A requirement for vectorial proton transport is that deprotonation and reprotonation of the Schiff base occur from the opposite sides of the membrane. The transition between these two different accessibilities is termed the "hydration switch". Because the M state is the only state in which the Schiff base is deprotonated, there must be two substates of M that differ in their accessibility and are, therefore, called M_{ec} (M with extracellular accessibility) and M_{cp} (M with cytoplasmic accessibility).[8−11]

Various biophysical methods have been used to characterize the photointermediate states in detail and to relate them to transport function (for reviews, see refs 3 and 12−15). The high-resolution crystal structures of the unilluminated state of the protein[16] and photointermediates[10,17−25] have supplied molecular details regarding the changes that occur in the configuration of the retinal upon illumination as well as the resulting conformational changes of the protein. In short, the structures show that on the extracellular side of the proton

Received: October 8, 2013
Revised: March 20, 2014
Published: March 24, 2014

   dx.doi.org/10.1021/bi4013808 | *Biochemistry* 2014, 53, 2380−2390

conducting pathway the ground-state Schiff base associates with a complex counterion composed of Asp85 and Asp212 through a highly polarized water molecule. Furthermore, a network of polar residues and bound water is thought to couple the protonation state of Asp85 to a complex proton release group (PRG) on the extracellular side.[26−32] One such residue, Arg82, has even been shown to alternate between upward- and downward-facing orientations during the photocycle and may thus serve a key role in shuttling protons between Asp85 and the PRG.[33−36] Structural changes in the cytoplasmic half-channel are initiated by the 13-methyl group of the retinal that pushes after isomerization and relaxation against the indole ring of Trp182.[35,37] This, and other molecular stresses, leads to a transient outward tilt of the upper part of helix F and an inward movement of helix G in the second half of the photocycle.[25,37] This helix repacking leads to the lowering of the pK_a of Asp96, which is initially high (>12), and the establishment of a hydrogen-bonded chain to the Schiff base, which together facilitate the reprotonation of the Schiff base from the cytosol.[10,38−41]

In a previous paper, we demonstrated that the transport activity of the bacteriorhodopsin Asp96Gly/Phe171Cys/Phe219Leu triple mutant is 66% that of the wild type in whole haloarchaeal cell measurements.[42] Surprisingly, substantial conformational changes were absent during the photocycle of this mutant given that its conformational ground state resembled that of the wild-type BR M conformation, which is called the open state.[43] Recently, a three-dimensional X-ray structure has been reported for the triple mutant. This structure suggests that the open state may be more even open than previously appreciated[25] (Figure S1). Accompanying molecular dynamics (MD) simulations in which the mutant residues were reverted back to wild type suggested that substrate access to the cytoplasmic half-channel is tightly regulated by the protonation state of Asp96, even in the structurally highly open conformation. This would indicate that although the large-scale structural change likely remains functionally important it alone is not sufficient to regulate substrate flow and that other mechanisms are also involved.

In this article, we demonstrate that haloarchaeal cells expressing the triple mutant BR can use light energy to synthesize 85% of the ATP synthesized by the wild-type protein but, nevertheless, they cannot grow photoheterotrophically. To resolve some of the seemingly contradictory functional results (e.g., the triple mutant pumps protons, cells expressing it make reasonable amounts of ATP, and this activity does not support growth) in the context of what we know about its structure, we expressed wild-type and mutant BR in *Xenopus* oocytes and examined the effect of membrane potential on the generation of light-induced proton current. We also conducted MD simulations to help provide dynamic structural context for the biophysical measurements. In so doing, we show that the constitutively open state of the triple mutant may make the protein nonfunctional at physiological membrane potentials by providing a route for substrate back flow in the presence of a inwardly negative membrane potential. This realization, in combination with alternate, non-BR-mediated routes for short-term light-driven ATP synthesis help to bring clearer focus on the functional potential of the triple mutant.

MATERIALS AND METHODS

ATP Measurements. Light-driven ATP synthesis rates were measured by growing halobacterial cells to the end of the logarithmic phase and then harvesting and resuspending the cells in basal salt (growth medium without peptone) at a pH value of 5.7.[44] Cellular ATP concentration was determined by a luciferin/luciferase assay (Sigma, product ID: FLAAM) according to the manufacturer's protocol. Photon emission was used as a measure of the ATP concentration (Lumac Biocounter, Abimed, Germany). Absolute ATP concentration was determined by comparison to a standard curve. The light-driven ATP synthesis rate was determined by illuminating the cell suspension with green light emitted from a halogen bulb-equipped slide projector. Projected light was filtered by a OG515 cutoff filter (Schott, Mainz, Germany) and a Calflex 3000 heat glass (Balzers, Liechtenstein) prior to sample illumination. The light intensity was 19.2 mW cm^{-2}. Light was switched on at time t = 0, and ATP concentration was determined as the mean value of triplicate samples taken at time points −600, −300, −5, 5, 15, 25, 35, 45, 60, 120, 180, 240, and 300 s. the ATP synthesis rate was calculated by linear regression of the five time points after switching on the light.

Gene Constructs. The wild-type and mutant bacterioopsin genes were cloned into pGEMHE, providing a multiple cloning site surrounded by the noncoding regions of β-globin from *Xenopus laevis*.[45] The DNA insert was generated by standard PCR.

Preparation of the Oocytes. After removal from the frog, ovarian lobes were cut into small pieces, washed three to four times in oocyte Ringer ORI (82.5 mM NaCl, 2.5 mM KCl, 1 mM $MgCl_2$, 1 mM Na_2HPO_4, and 5 mM HEPES, pH 7.4) and subjected to collagenase treatment (approximately 0.5 μg/mL of collagenase A (Sigma) depending on the lot) in ORI for 4 to 5 h. Thereafter, the oocytes were washed thoroughly with ORI medium and stored for further treatment in ORI II buffer (82.5 mM NaCl, 2.5 mM KCl, 1 mM $MgCl_2$, 1 mM Na_2HPO_4, 1 mM $CaCl_2$, 1 μg/mL of sodium pyruvate, 50 ng/mL of gentamycin (Boehringer), and 5 mM Hepes, pH 7.4) at 18 °C in the dark.

Expression in *Xenopus laevis*. Plasmids were linearized using the restriction enzyme *Pst*I and treated with Klenow fragment I to eliminate the 3′ overhang. Capped cRNA was produced in an *in vitro* transcription reaction using T7 RNA polymerase (New England Biolabs). After injection of 50 −100 ng of cRNA, the oocytes were incubated in the dark at 18−20 °C for 3 to 4 days in ORIII solution additionally containing 1 μM all-trans retinal for reconstitution of bacteriorhodopsin.

Protein Quantification. Ten to 15 oocytes were homogenized in 1 mL HOMO buffer (0.1 mM DTT, 1 mM PMSF, and 10 mM Tris/HCl, pH 8). The homogenate was centrifuged to pellet the nuclei (10 min, 4 °C, 2700g). The supernatant was then subjected to an ultracentrifugation at 100 000g for 45 min at 4 °C to pellet the membrane fraction. This pellet was washed with HOMO buffer and solubilized in 10 μL/oocyte of RIPA buffer (1% Triton X-100, 1% Na deoxycholate, 0.1% SDS, and 20 mM Tris/HCl, pH 7.3).

Approximately 1−5 μg of protein was separated on a 13% SDS polyacrylamide gel (PAGE) and blotted onto a nitrocellulose membrane. Bacterioopsin (BO) was visualized using a BO antibody[46] and the ECL immuno-staining kit (Amersham, Freiburg, Germany). For quantification, each gel was calibrated with known amounts of BO. Signal intensities were calculated using the ImageJ software package (http://rsb.info.nih.gov/ij).

Electrophysiological Measurements. Two-electrode voltage-clamp experiments were performed using a GeneClamp500 amplifier and the pClamp7 software package (Axon Instruments). The measurements were performed in a bath

solution containing 80 mM NaCl, 3 mM NaN_3, 10 mM CsCl, 10 mM TEACl, 5 mM $BaCl_2$, 2 mM $CaCl_2$, 2.5 mM Na-pyruvate, and 10 mM MES, pH 5.5. Actinic light was produced from a mercury arc lamp (HBO 300 Oriel, Darmstadt, Germany) that was filtered by an OG515 cutoff (Schott, Mainz Germany) and a heat glass (Balzers, Liechtenstein) and applied via fiber optics. The light intensity at the cuvette surface was 16.3 mW cm^{-2}. Data were filtered at 10 Hz and were further processed (data reduction) before extracting the photocurrent from whole cell currents. The photocurrents were extracted from the raw data by calculating the difference between the linear approximation of the dark current and the current during illumination. The leak conductance of the measurements was typically in the range of 1−10 mS. The access resistance was 5−15 MΩ.

Molecular Dynamics Simulations. Two sets of molecular dynamics simulations were performed starting from the X-ray crystal structure of the triple mutant (PDB ID: 4FPD).[25] In the first set of five replicates simulations (named G1−G5), the protonation states of the ionizable residues were set as in the ground state (i.e., Asp85 and Asp212 were deprotonated, and Asp115 was protonated). In the second set of three replicates simulations (name M1−M3), Asp85 was modeled in the protonated state to mimic the M intermediate state (residue Asp115 remained protonated, and Asp212 remained deprotonated). In addition, three replicates simulations were performed starting from the earlier low-resolution electron microscopy (EM) structure of the triple mutant (PDB ID: 1FBK),[43] and in these simulations, D85 was modeled in the protonated state. In each simulation, the BR protein was embedded in a phospholipid bilayer of palmitoyloleoyl-phosphatidylcholine (POPC) and solvated in water with an ion concentration of 200 mM (the concentration was selected on the basis of previous experiments that (a) determined 1 M to be a practical upper bound for accurately modeling ionic composition,[47] (b) our own previous comparison between 200 mM and 1 M ionic concentrations,[25] and (c) the functional observation that BR retains function at these relatively low ionic strengths).

The detailed methods for modeling the BR proteins in the solvated membrane environment were previously described.[48] All of the MD simulations were carried out using the GPU-CUDA version of the AMBER11 program of the Amber biomolecular simulation programs.[49] The protocol for setting up the MD simulations, including energy minimization, equilibration, and product run, was previously described.[48] We highlight a few key parameters: The parameters of the POPC lipid molecules were taken from our previous work,[50] which were derived by using the Antechamber module and GAFF force field in the AMBER program. The parameters of protein residues were assigned on the basis of the AMBER ff03 force field,[51] a point-charge force field for molecular mechanics simulations of proteins based on condensed-phase quantum mechanical calculations. For water molecules, the TIP3P model was used. The simulations range from 224.01 to 753.92 ns for a total of 4.0 μs.

Water Channel Analysis. We analyzed water occupancy in the cytoplasmic proton uptake channel, which we defined as the cavity between Asp96 and Lys216. This cavity is approximated by a sphere that is centered at the midpoint of the line connecting the Gly96:CA and Lys216:CA atoms. The radius of the sphere was set to be the half of the distance between those two atoms minus 1 Å. In the triple-mutant structure (PDB ID: 1FPD), the distance between the Gly96:CA and Lys216:CA atoms is 11.52 Å, and there is only one crystal water molecule located in the cavity. For each simulation trajectory, we computed the number of the water molecules present in the cavity at every frame. Increases in the number of water molecules present in the cavity is used as a proxy for the formation of a water channel. From prior experience, we set the cutoff as 4; that is, when the number of water molecules is larger than 4, we considered the channel to be open. In addition, we analyzed the dynamic exchange of the channel water molecules with the bulk by computing the total number of unique individual water molecules that ever access the G96-K216 cavity during the simulation. Lastly, the water channel was visualized with the MolAxis program.[52]

RESULTS

ATP Synthesis. The report demonstrating proton transport activity in the Asp96Gly/Phe171Cys/Phe219Leu mutant of BR in the absence of a significant conformational change[42] raised the question about whether the mutant's activity could be physiologically functional in the cell. Namely, could the transport activity generate sufficient proton motive force to measurably increase the cellular ATP synthesis rate in response to light? To answer this, light-induced ATP synthesis rates were determined in *Halobacterium salinarum* cells expressing either wild-type or triple-mutant BR.

ATP levels were measured in cells prior to illumination (negative time points in Figure 1A) and at time points up to 300 s postillumination. In both wild-type (Figure 1A) and triple-mutant BR (Figure 1B), the ATP levels increased and leveled off after 120 s. The initial ATP synthesis rate was determined by regression analysis (dotted lines in Figure 1A,B) through the linear range (45 s after light on). Wild-type and triple mutant rates were 0.095 and 0.082 nmol ATP/BR, respectively. The initial light intensity was 19.2 mW cm^{-2}. To ensure that the ATP synthesis rates were not measured under conditions that saturated the ATP synthase, the experiments were repeated at different light intensities.[53] As shown in Figure 1C, a clear dependence of the ATP synthesis rates on the applied light intensities was found. Therefore, light-induced ATP-synthase saturation was excluded, and we presumed that the measured ATP synthesis rates reflected the increased proton motive force by the activity of BR in wild-type as well as in the triple-mutant cells.

In a second experiment, cells expressing the triple mutant were exposed to photoheterotrophic growth conditions. In contrast to wild-type cells, mutant cells did not grow under these conditions and all others tested (see the Discussion). This indicates that the increased ATP synthesis rates that were found in the time range of 300 s were nevertheless not sufficient to maintain the required ATP levels for cellular growth.

The BR content in halobacterial cells was determined spectroscopically after the lysis of the cells and preparation of the total membrane fraction. For BR, a molar extinction coefficient of 63 000 M^{-1} cm^{-1} was used, and scattering was corrected by assumption of a standard scattering curve. This method is used routinely in the lab and turned out to be sufficient for determining BR abundance.

Expression in Oocytes. To understand the function of an ion transport protein fully, it is critical to know its current−voltage relationship (e.g., the current that the protein can generate in the context of varying transmembrane voltages). For context, the previously reported light-induced proton-pumping activities of BR and its mutants were measured in

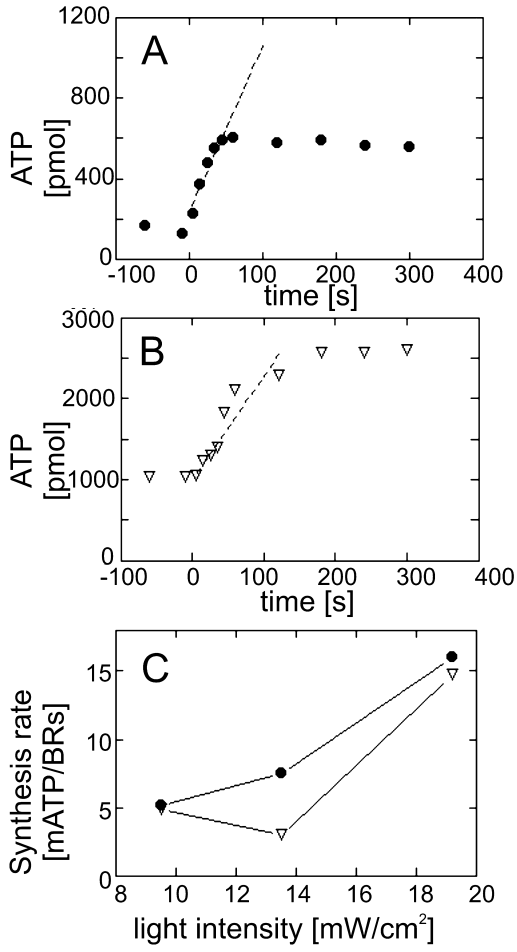

Figure 1. Light-induced change of ATP concentration in halobacterial cells containing (A) wild-type BR (strain S9) or (B) mutant BR (strain TOM, two opsin minus, derived from L33 expressing the triple mutant from a plasmid). Data points shown represent the mean value of three independent determinations. The standard deviations were less than 10% for all data points; therefore, the error bars are not shown. For determination of the initial ATP synthesis rate, the linear regression of the first five data points was calculated, and the result is indicated by the dashed lines. (C) Dependence of the ATP synthesis rate on different light intensities. Note that the *y*-axis scale in panels A and B are different.

haloarchaeal cells under conditions of zero membrane potential (short-circuit conditions) by addition of 200[54] or 400 μM[42] tetraphenylphosphonium (TPP). Because of their small size, haloarchaeal cells were not suitable for manipulations with microelectrodes for electrophysiological experimentation. Therefore, a heterologous expression system (oocytes) had to be used.

Quantification of Expression. As was shown by the pioneering work of Bamberg and colleagues,[55−57] functional expression of BR in oocytes allows direct measurement of the voltage dependence of light-induced proton pumping. Microinjection of wild-type or mutant mRNA into oocytes led to expression of the respective BR molecule in the cell membrane of oocytes as detected by western blot analysis. Total membrane fractions from 10 oocytes were separated by SDS-PAGE, transferred to a nylon membrane, and incubated with an antibody to bacterioopsin. A clear band with an apparent molecular weight of 19 kD was identified for expressed wild-type as well as mutated BR (Figure 2A, lanes 5 and 6). For quantitation, increasing amounts of BR, 12.5, 18.8, 25, and 32.2 ng from purple membranes, were electrophoresed on the same gel (Figure 2A, lanes 1−4). Densitometric analysis of lanes 1−6 is shown in Figure 2B, and the integrals of the traces were subjected to regression analysis (Figure 2C). All values fell on a straight line, so the expression values of 75 and 42 ng for wild-type and mutant BR, respectively, were directly determined. This corresponds to 0.25 and 0.14 pmol per oocyte. In different expression experiments, a range from 0.11 to 0.56 pmol per oocyte was found. For the sake of clarity, the following calculations were done for the wild type value. The value of 0.25 pmol corresponds to 1.5×10^{11} molecules per oocyte. Assuming a surface area for the oocyte of 20 mm^2,[58] a density of 7500 molecules μm^{-2} is calculated. This is roughly five times lower than the density of BR in the haloarchaeal cell, where as many as 600 000 molecules per cell are distributed on a surface of 15 μm^2.

Electrophysiological Experiments. The ability of wild-type BR and the triple mutant to generate light-induced currents against various transmembrane potentials (i.e., the current−voltage (*IV*) relationship) was determined by patch clamping these proteins after heterologous expression in oocytes. Average current recordings of wild-type (n = 18) and mutant BR (n = 19) are reported in Figure 3, panels A and B, respectively. Voltages, varying from −150 (bottom) to +50 mV (top), were applied for 6 s. This process began 1 s after the start of each experiment when the membrane potential was set to a defined holding potential. After the current stabilized (ca. 2.5 s), samples were irradiated with a 1 s pulse of actinic light. The current usually returned to the t = 0 value following the light pulse. After 4 s, the holding membrane potential was switched off.

Because the opsins are the only light-induced transport system in the oocytes, the difference in current at fixed membrane potentials between the stationary photoinduced current and the dark current can be attributed to the activity of the opsin proteins. Plotting these opsin-associated currents versus the applied membrane potential shows the stationary current−voltage (*IV*) relationship of each opsin. Figure 4A,B reports these data for wild-type and triple-mutant BRs, respectively. First, we note that only positive photoinduced currents were measured for both wild-type and triple-mutant BR, indicating that reversal of the pump was not observed. Second, the currents driven by wild-type BR are larger than the currents from the triple mutant. Note that the ordinates in panels A and B are scaled differently and that the currents were normalized to the amount of expressed protein. Third, the *IV* curve of the triple mutant BR is nonlinear (convex), whereas that of the wild type was only slightly nonlinear and concave. In conclusion, the currents in wild type are 10 times higher at −150 mV compared to the mutant, but this value reduces to five times higher at +40 mV because of the nonlinear characteristic of the current−voltage relationship.

The physiological relevance of current−voltage relationships determined for oocyte-expressed BR was assessed and reported in previous work using the same methods.[59] Therein, current−voltage curves of wild-type BR expressed in oocytes showed the BR turnover rate in the oocyte to be about 1 s^{-1} at zero membrane potential. This value is very close to the experimentally determined value of 5 H$^+$/BR s^{-1} for the maximal transport rate of BR in the halobarchaeal cell.[42] Moreover, if one considers that previous experiments using the oocyte system suggested that only 10% of the translated BRs

dx.doi.org/10.1021/bi4013808 | *Biochemistry* 2014, 53, 2380−2390

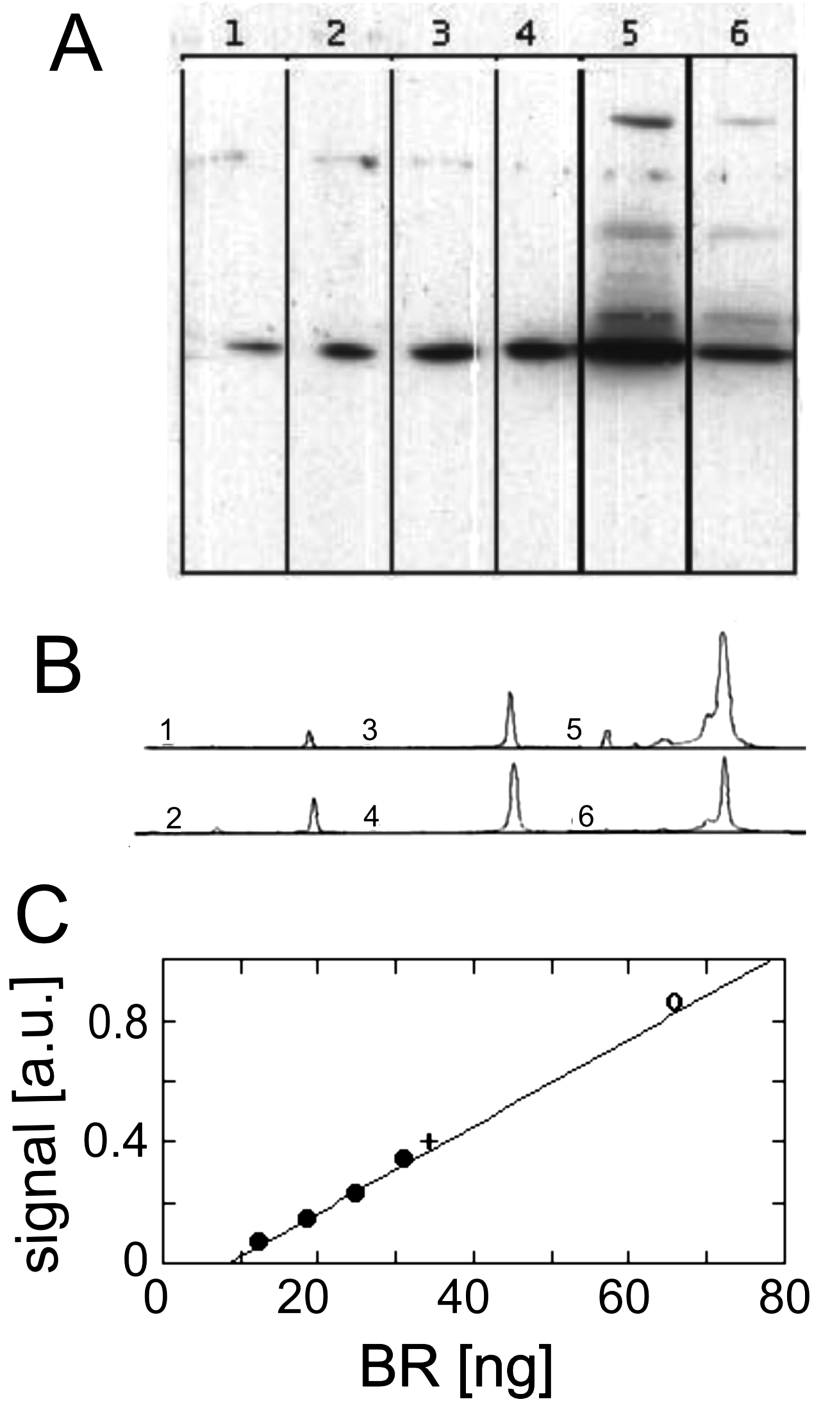

Figure 2. Quantification of expression of wild-type and mutant BR in oocytes. (A) Western blot of total membrane fractions of wild-type (lane 5) or mutant (lane 6) BR-expressing oocytes. In lanes 1−4, 12.5, 18.8, 25, and 32.2 ng of BR were applied for calibration, respectively. (B) Densitograms of lanes 1−6. (C) Regression analysis of the integrals of the curves shown in panel B (standard values, dots; wild-type BR, open circle; and mutant BR, cross).

actually appear in the plasma membrane,[57] then the turnover in oocytes from 1 to 10 s^{-1} is closer still to the value of 5 s^{-1} reported in halobarchaeal cells.

Molecular Dynamics Simulations. To provide mechanistic context for our current−voltage data, we analyzed the X-ray structure of the triple mutant[25] and conducted a series of molecular dynamics simulations. The 2.65 Å structure of the triple mutant is characterized by large displacements of the cytoplasmic ends of helices E, F, and G (Figure S1). The largest displacement from the wild-type ground-state structure is a 14.7° outward tilt of helix F that initiates at Pro186. Notably, despite this large tilt, solvent-accessible surface calculations show that in the static structure the proton uptake pathway remains functionally closed. That is, access of bulk water to the cytoplasmic interior extends only to Phe42, which, along with a hydrophobic leucine ring (Figure S2), appears to act as a cap for the cytoplasmic half-channel.

For this study, a total of eight simulations, termed G1−5 (modeling ground state) and M1−3 (modeling an M-like state), were conducted with starting atomic coordinates derived

dx.doi.org/10.1021/bi4013808 | *Biochemistry* 2014, 53, 2380−2390

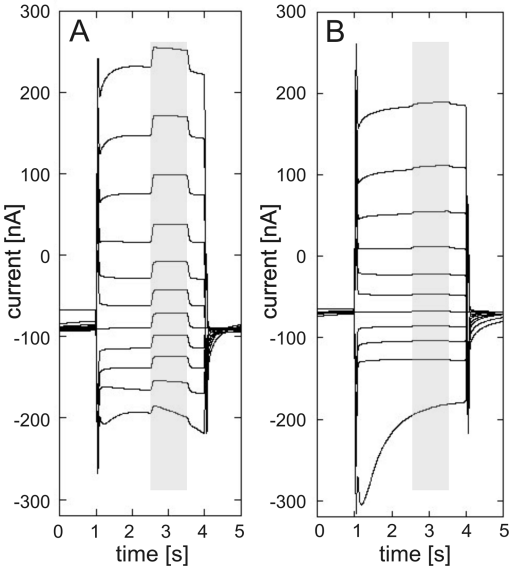

Figure 3. Averaged current recordings of oocytes expressing (A) wild-type BR (n = 18) or (B) mutant BR (n = 19). Voltages are applied in the range of −150 to 50 mV in 20 mV increments from bottom to top. A 1 s light pulse (source: HBO 300, Oriel filtered through OG515, Schott and Calflex 3000, Balzers, 16.3 mW cm^{-2}) was applied between 2.5 and 3.5 s. The rough illumination region is depicted with a gray rectangle. The bath solution contained 80 mM NaCl, 3 mM NaN_3, 10 mM CsCl, 10 mM TEACl, 5 mM $BaCl_2$, 2 mM $CaCl_2$, 2.5 mM Na-pyruvate, and 10 mM MES at pH 5.5; electrodes were filled with 3 M KCl.

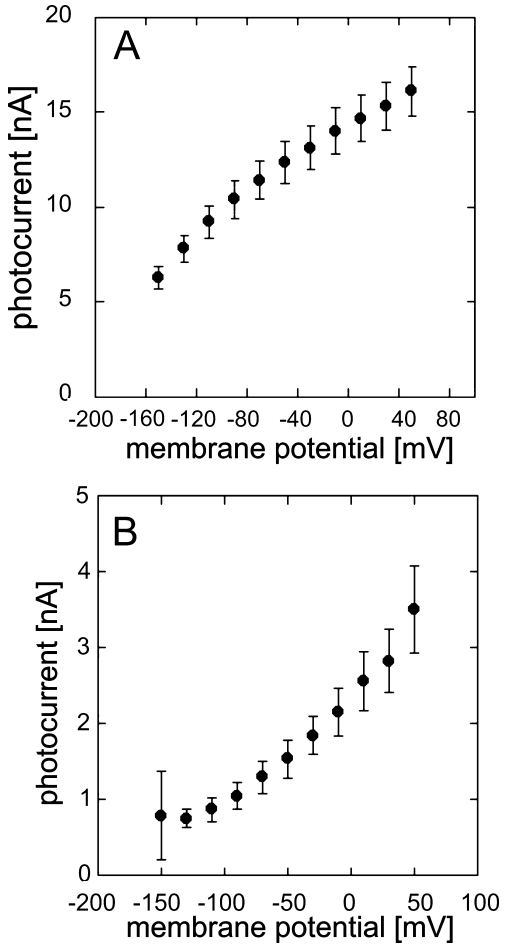

Figure 4. Averaged current−voltage relationship of wild-type BR (A) and mutant BR (B) from 18 and 19 independent measurements, respectively, as shown in Figure 3. The standard deviation is indicated by the bars. Experimental conditions were as described in Figure 3. Note that the y axis in panels A and B is on different scales.

from 4FPD. In seven of the eight simulations, we observed that a water channel readily formed along the putative proton uptake pathway, connecting the backbone carbonyl group of Lys216 (and thus possibly the Schiff base during the M-to-N transition and N-intermediate) and the cytoplasm. The opening was created by the outward swinging of Phe42 and loosening of the packing of the leucine-rich cluster around Gly96. This opening was characterized by an increase in the distance between Phe42 and Gly96 and the increase of the radius of gyration of the leucine-rich cluster, which led to a dramatic increase in the number of water molecules in the Gly96−Lys216 cavity (Figures 5 and S3). As described in the Water Channel Analysis section of the Materials and Methods, four or more water molecules present in the cavity indicates the formation of the water channel. Charged residues including Arg227 at the C-terminal of helix G, Asp38 and Lys41 of helix B, and Asp102 at loop BC lined the entrance of the channel. In the open state, water molecules filled the cytoplasmic channel and underwent rapid and dynamic exchange with the bulk (Figures 5 and S3 and Table 1). In the region around Gly96, the channel was bottlenecked to a narrow gate with a diameter of 2−2.5 Å, allowing only one water molecule to pass at a time between the exterior and interior portions of the cytoplasmic half-channel (the pink pipe shown in Figure 6). The location of the channel determined in these simulations is the same as the one previously reported from simulations of wild-type BR in which D96 was modeled in the deprotonated state.[25]

The formation of the water channel exhibited different kinetics and dynamics in different simulations. In simulations G1, G2, and G4, the water channel formed almost immediately after the restraints on the protein were removed, whereas in simulations M1, M2, and M3, it took several tens of nanoseconds. The slowest opening occurred in simulation G5, which took ca. 450 ns. In most of the simulations, we observed that the protein spontaneously alternated between the channel opened and closed conformations, as characterized by the rapid fluctuation of the number of water molecules in the Gly96−Lys216 cavity (Figures 5 and S3). By contrast, in simulations G2 and G5, the channel reclosed, and the closed state lasted until the end of the simulations. In simulation G2, the number of the water molecules in the Gly96−Lys216 cavity dropped back to one after about 5 ns because Leu219 was kicked into the Gly96−Lys216 cavity by a surrounding lipid molecule (Figure S4). In simulation G5, the open state lasted for only 100 ns, and the channel closed as a result of Phe42 rotating back to cover Gly96. Simulation G3 was the only simulation in which the proton uptake channel never opened but a few water molecules penetrated into the protein from the transiently created cavity between helices B and G (Figure S5)

A second, lower-resolution structure of the triple mutant determined by electron diffraction (PDB ID: 1FBK) was also used to simulate an M-like state in the triple mutant. The EM structure is also characterized by helical tilts on the cytoplasmic side of the protein. However, the structural deviations relative to the wild-type ground-state BR structure are generally smaller in 1FBK than they are in 4FPD: the outward tilts of helix F in

dx.doi.org/10.1021/bi4013808 | Biochemistry 2014, 53, 2380−2390

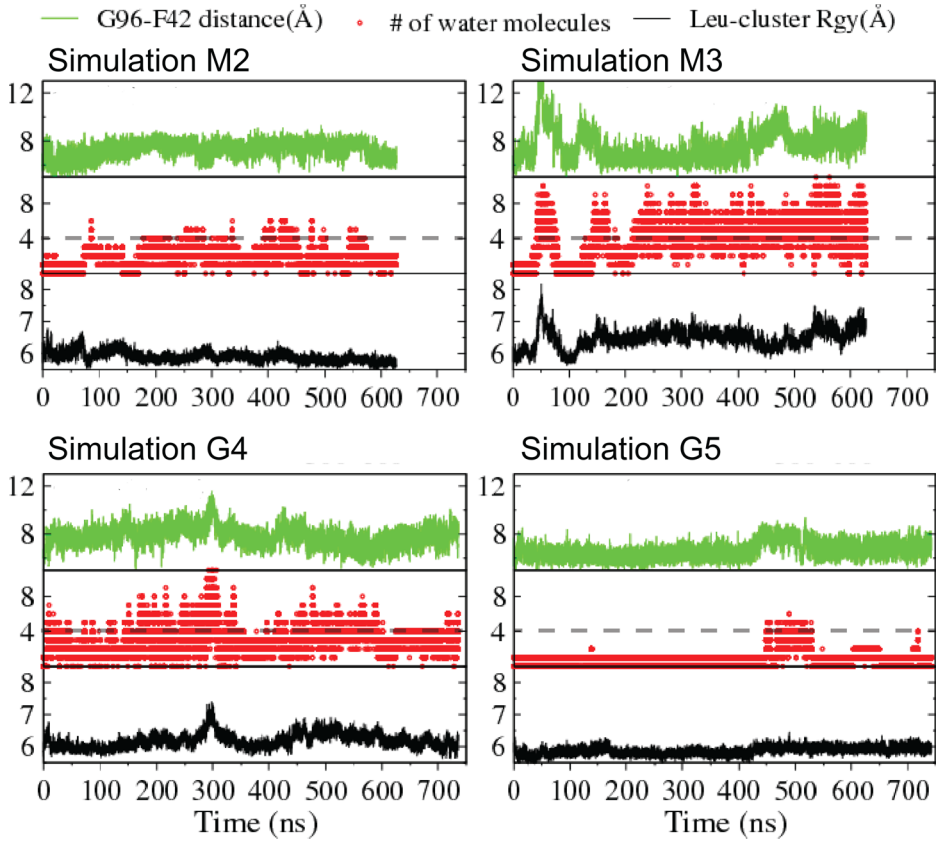

Figure 5. Dynamics in the vicinity of Gly96 in four of the simulations starting structure 4FPD. For each simulation, the Gly96−Phe42 side chain Cα−Cg distance (green), the number of water molecules in the Gly96−Lys216 cavity (red), and the radius of gyration of the leucine-rich cluster (black) are each plotted against the simulation time. A horizontal dashed line indicates 4 water molecules, the threshold value for defining an open channel. See Figure S3 for the other four simulations.

Table 1. Summary of the MD Simulation Results

simulation	state[a]	trajectory length (ns)	number of different water molecules that accessed the G96-K216 cavity
Eight Simulations Starting from Structure 4FPD			
G1	ground	289.38	363
G2	ground	256.48	32
G3	ground	530.12	12
G4	ground	753.92	774
G5	ground	753.92	43
M1	M	626.88	877
M2	M	627.01	106
M3	M	627.01	883
Three Simulations Starting from Structure 1FBK			
E1	ground	229.01	3
E2	ground	229.01	23
E3	ground	224.11	13

[a]D85 is protonated in the simulations mimicking the ground state and deprotonated in those mimicking the M state.

4FPD and 1FBK are ∼15 and ∼6°, respectively (Figure S1). To investigate whether the differences in starting states might influence the simulation results, we conducted three additional MD simulations with protonatable residues modeled in M-like states. In contrast to the simulations conducted on 4FPD, the proton uptake channel remained closed in each of the three simulations that started from 1FBK (simulations E1−E3). In these simulations, a few water molecules penetrated into the protein from the transiently created cavity between helices B and G (Figure S6). This behavior is similar to what was seen in simulation G3 and suggests that the water channel observed in simulations based on the 4FPD structure is unlikely to be observed in the simulation based on the 1FBK structure. Although both 4FPD and 1FBK model the BR triple mutant structure in the ground state, different experimental approaches and conditions led to notably different structures and apparently different stabilities of the cytoplasmic half-channel. This suggests that factors that influence the degree of opening on the cytoplasmic side of the triple mutant may modify the transport kinetics.

DISCUSSION

Analysis of the triple mutant structure and the accompanying molecular dynamics simulations reveal that the constitutively open cytoplasmic side of the triple mutant may help to explain both its ability to pump protons (reprotonate the Schiff base) in the absence of the internal proton donor Asp96 and its inability to pump against a physiologically relevant negative membrane potential. Each of these two phenomena can be directly linked to the dynamic hydration of the cytoplasmic half-channel. In the case of the former, direct hydration of the Schiff base from the cytoplasmic bulk provides a path for reprotonation. This hypothesis is supported by the experimental observation that the reprotonation rate of the Schiff base is pH-dependent in the triple mutant,[42] in contrast to the external pH-independent manner of the wild type. Likewise, the increased hydration provides a low resistance route for

dx.doi.org/10.1021/bi4013808 | Biochemistry 2014, 53, 2380−2390

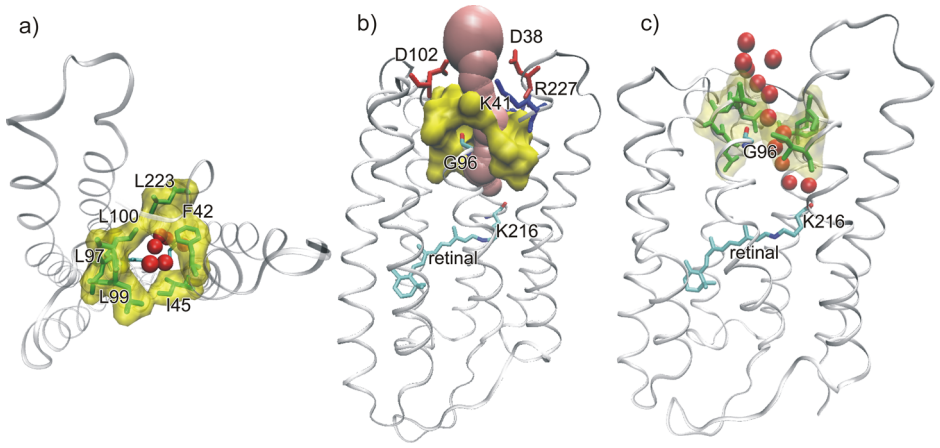

Figure 6. Representative conformation of the open proton uptake channel. (A) Model viewed from the CP side. Six water molecules (red balls) are shown in the Gly96−Lys216 cavity. The opening is surrounded by a leucine-rich hydrophobic cluster formed by Phe42, Ile45, Leu97, Leu99, and Leu223 (green stick and yellow surface); (B, C) side view. The pink pipe depicts a contiguous water channel that connects the cytoplasm with Lys216 and passes by Gly96.

substrate back flow, particularly when the direction of pumping is energetically contrary to the membrane potential.

In a recent paper by Geibel et al.,[60] the authors report photocurrents for the triple mutant (as well as the respective single mutations) expressed in the oocyte expression system. In addition to the photocurrents triggered by actinic green light, the authors also report the response of the triple mutant to flashes of blue light pulsed at intervals after a stimulus by green light. These experiments showed that the lifetime of the M intermediate is prolonged in Asp96Gly and the triple mutant but shortened in the Phe171Cys and Phe219Leu mutants. All of these experiments were carried out at pH 7.5. A comparison of the electrical data presented herein with those of Geibel et al.[60] shows agreement of the current−voltage curves in the triple mutant. We note, however, that our measurements were performed at pH 5.5 and that because of the absence of Asp96 as the intrinsic proton donor for reprotonation of the Schiff base the BR photocycle, especially the M decay component, is highly pH-dependent in these mutants. Lastly, we also note that the observation of Geibel at al.[60] that the blue light response changes its sign exclusively in the triple mutant could be interpreted as an indication that this mutant has altered the directionality of proton currents and that this would be compatible with our suggestion of back flow under conditions of positive potential.

It is worth noting that the dynamics of water molecules in the cytoplasmic half-channel described above are in sharp contrast to the MD simulations recently published by Wang et al.[25] in which residues in the triple mutant (PDB ID: 4FPD) were returned *in silico* to the wild-type BR identities. The simulations in Wang et al. preserve the large structural change observed in the mutant while probing the role of wild-type side chain chemistry in that context. Surprisingly, even in the open state, the wild-type substitutions serve to control access to the cytoplasmic half-channel despite the presence of large-scale conformational changes. Only when Asp96 is modeled in a deprotonated state does the cytoplasmic half-channel open to allow rapid water exchange, not unlike that seen in the present study. The apparent design feature, which requires complex molecular control of hydration on the cytoplasmic side (e.g., the large-scale changes are insufficient), suggests moreover that this functional property has been honed carefully by natural selection and that it is critical for the proper function of the pump. The opening appears to be timed to occur well after proton transfer from the Schiff base (a process that may be mediated by a chain of water molecules not unlike those observed in this study[41]) linked to the protonation state of Asp96 and exists only long enough to fulfill the function of reprotonating Asp96.

Understanding that the perpetually open cytoplasmic half-channel (mediated by the absence of an ionized Asp96 in the triple mutant) may contribute to back flow when the mutant pump is operating against a transmembrane potential, which may also provide some explanation for the previously contradictory results: (a) proton pumping by the triple mutant shows 66% of wild-type efficiency[42] and (b) the inability of cells expressing the triple mutant to sustain photoheterothrophic growth. First, we note that pumping efficiency data were collected in the presence of high concentrations of the lipophillic cation tetraphenylphosphonium (TPP). This compound effectively set the membrane potential to zero, which was useful for comparing wild-type and mutant internal thermodynamics but masked the inability of the mutant to pump against a voltage. Second, the conclusion that cells expressing the triple mutant, which we have now shown to be effectively nonfunctional at physiological membrane potentials, cannot grow photoheterotrophically is consistent with previous data showing that cells lacking a functional BR can likewise not sustain photoheterotrophic growth.[61−64]

What remains unanswered by the current work, however, is the data showing light-mediated ATP synthesis in double knockout cells lacking wild-type BR or halorhodopsin but expressing the triple mutant. If the triple mutant proton pump is nonfunctional at physiological membrane potentials, then how can it still seemingly mediate light-dependent ATP synthesis? Previous work had implicated the membrane potential established by the light-mediated activity of halorhodopsin (the inward-driven Cl^- transporter) in the synthesis of ATP in *H. salinarum* mutants lacking functional BR.[61−63] This halorhodopsin activity was similarly implicated as a primary driver of light-driven ATP synthesis in haloarchaeal species lacking BR.[65] However, cells utilized in this study lack functional halorhodopsins. Previous work has shown light-dependent ATP synthesis in the absence of a proton motive

dx.doi.org/10.1021/bi4013808 | *Biochemistry* 2014, 53, 2380−2390

force, although the mechanism by which this happens remains unclear.[66] Thus, we suggest that the observed initial ATP production is only transient in the mutant in contrast to the situation in wild-type cells. Photoautotrophic growth would require steady-state ATP production, as has been demonstrated previously by growth deficiencies in BR-minus strains.[64]

Collectively, the new current−voltage data for the triple mutant and their analysis in the context of protein structure and MD simulations helps to explain some of the seeming contradictions of previous experimental data on this protein. These results also reinforce the notion that minimizing the potential for back flow is a critical element in the design of BR that is tightly regulated. The structural opening that occurs during the late M and N photointermediates likely serves to mediate a temporary increase in channel hydration, whereas the closing is required to minimize the potential for back flow when pumping against physiological membrane potential.

■ ASSOCIATED CONTENT

Supporting Information

The Supporting Information include graphical summaries of key data derived from MD simulation trajectories and cartoon style diagrams of protein structures that depict the starting X-ray crystal structures used in the MD simulations and snapshots of particularly illustrative structures derived from MD simulations. This material is available free of charge via the Internet at http://pubs.acs.org.

■ AUTHOR INFORMATION

Corresponding Author

*Tel.: 530-752-3781; E-mail: mtfacciotti@ucdavis.edu.

Author Contributions

§T.W. and C.O. contributed equally to this work.

Funding

This work was funded by SFB533, the Ministry of Science and Technology of China (CB2013910200 to Y.D.), and the National Institutes of Health (GM67168 to Y.D.) as well as by computing resources at the TeraGrid (MCA06N028 to Y.D. and MCB100132 to T.W.) and startup funds to M.T.F.

Notes

The authors declare no competing financial interest.

■ ACKNOWLEDGMENTS

We thank E. Bamberg for helpful discussions and S. Subramaniam and A. K. Werenskiold for critical reading of early manuscript drafts. Skillful technical assistance from B. Brustmann is acknowledged.

■ REFERENCES

(1) Lozier, R. H., Bogomolni, R. A., and Stoeckenius, W. (1975) Bacteriorhodopsin: A light-driven proton pump in *Halobacterium halobium*. *Biophys. J. 15*, 955−962.

(2) Oesterhelt, D., and Stoeckenius, W. (1971) Rhodopsin-like protein from the purple membrane of *Halobacterium halobium*. *Nature, New Biol. 233*, 149−152.

(3) Haupts, U., Tittor, J., and Oesterhelt, D. (1999) Closing in on bacteriorhodopsin: Progress in understanding the molecule. *Annu. Rev. Biophys. Biomol. Struct. 28*, 367−399.

(4) Heberle, J. (2000) Proton transfer reactions across bacteriorhodopsin and along the membrane. *Biochim. Biophys. Acta 1458*, 135−147.

(5) Lanyi, J. K. (2004) Bacteriorhodopsin. *Annu. Rev. Physiol. 66*, 665−688.

(6) Lanyi, J. K. (2006) Proton transfers in the bacteriorhodopsin photocycle. *Biochim. Biophys. Acta 1757*, 1012−1018.

(7) Hirai, T., Subramaniam, S., and Lanyi, J. K. (2009) Structural snapshots of conformational changes in a seven-helix membrane protein: Lessons from bacteriorhodopsin. *Curr. Opin. Struct. Biol. 19*, 433−439.

(8) Kandori, H. (2004) Hydration switch model for the proton transfer in the Schiff base region of bacteriorhodopsin. *Biochim. Biophys. Acta 1658*, 72−79.

(9) Kataoka, M., Kamikubo, H., Tokunaga, F., Brown, L. S., Yamazaki, Y., Maeda, A., Sheves, M., Needleman, R., and Lanyi, J. K. (1994) Energy coupling in an ion pump. The reprotonation switch of bacteriorhodopsin. *J. Mol. Biol. 243*, 621−638.

(10) Schobert, B., Brown, L. S., and Lanyi, J. K. (2003) Crystallographic structures of the M and N intermediates of bacteriorhodopsin: Assembly of a hydrogen-bonded chain of water molecules between Asp-96 and the retinal Schiff base. *J. Mol. Biol. 330*, 553−570.

(11) Haupts, U., Tittor, J., Bamberg, E., and Oesterhelt, D. (1997) General concept for ion translocation by halobacterial retinal proteins: The isomerization/switch/transfer (IST) model. *Biochemistry 36*, 2−7.

(12) Herzfeld, J., and Lansing, J. C. (2002) Magnetic resonance studies of the bacteriorhodopsin pump cycle. *Annu. Rev. Biophys. Biomol. Struct. 31*, 73−95.

(13) Hirai, T., and Subramaniam, S. (2009) Protein conformational changes in the bacteriorhodopsin photocycle: Comparison of findings from electron and X-ray crystallographic analyses. *PLoS One 4*, e5769-1−e5769-16.

(14) Gerwert, K., Freier, E., and Wolf, S. (2014) The role of protein-bound water molecules in microbial rhodopsins. *Biochim. Biophys. Acta 1837*, 606−613.

(15) Kandori, H. (2000) Role of internal water molecules in bacteriorhodopsin. *Biochim. Biophys. Acta, Bioenerg. 1460*, 177−191.

(16) Luecke, H., Schobert, B., Richter, H. T., Cartailler, J. P., and Lanyi, J. K. (1999) Structure of bacteriorhodopsin at 1.55 Å resolution. *J. Mol. Biol. 291*, 899−911.

(17) Edman, K., Nollert, P., Royant, A., Belrhali, H., Pebay-Peyroula, E., Hajdu, J., Neutze, R., and Landau, E. M. (1999) High-resolution X-ray structure of an early intermediate in the bacteriorhodopsin photocycle. *Nature 401*, 822−826.

(18) Royant, A., Edman, K., Ursby, T., Pebay-Peyroula, E., Landau, E. M., and Neutze, R. (2000) Helix deformation is coupled to vectorial proton transport in the photocycle of bacteriorhodopsin. *Nature 406*, 645−648.

(19) Rouhani, S., Cartailler, J. P., Facciotti, M. T., Walian, P., Needleman, R., Lanyi, J. K., Glaeser, R. M., and Luecke, H. (2001) Crystal structure of the D85S mutant of bacteriorhodopsin: Model of an O-like photocycle intermediate. *J. Mol. Biol. 313*, 615−628.

(20) Sass, H. J., Büldt, G., Gessenich, R., Hehn, D., Neff, D., Schlesinger, R., Berendzen, J., and Ormos, P. (2000) Structural alterations for proton translocation in the M state of wild-type bacteriorhodopsin. *Nature 406*, 649−653.

(21) Facciotti, M. T., Rouhani, S., Burkard, F. T., Betancourt, F. M., Downing, K. H., Rose, R. B., McDermott, G., and Glaeser, R. M. (2001) Structure of an early intermediate in the M-state phase of the bacteriorhodopsin photocycle. *Biophys. J. 81*, 3442−3455.

(22) Chen, D., and Lanyi, J. K. (2009) Structural changes in the N and N′ states of the bacteriorhodopsin photocycle. *Biophys. J. 96*, 2779−2788.

(23) Lanyi, J. K., and Schobert, B. (2006) Propagating structural perturbation inside bacteriorhodopsin: Crystal structures of the M State and the D96A and T46V mutants. *Biochemistry 45*, 12003−12010.

(24) Lanyi, J. K., and Schobert, B. (2007) Structural changes in the L photointermediate of bacteriorhodopsin. *J. Mol. Biol. 365*, 1379−1392.

(25) Wang, T., Sessions, A., Lunde, C., Rouhani, S., Glaeser, R., Duan, Y., and Facciotti, M. T. (2013) Deprotonation of D96 in bacteriorhodopsin opens the proton uptake pathway. *Structure 21*, 290−297.

(26) Sasaki, J. (1995) Glutamic acid 204 is the terminal proton release group at the extracellular surface of bacteriorhodopsin. *J. Biol. Chem. 270*, 27122−27126.
(27) Rammelsberg, R., Huhn, G., Lübben, M., and Gerwert, K. (1998) Bacteriorhodopsin's intramolecular proton-release pathway consists of a hydrogen-bonded network. *Biochemistry 37*, 5001−5009.
(28) Balashov, S. P., Lu, M., Imasheva, E. S., Govindjee, R., Ebrey, T. G., Othersen, B., Chen, Y., Crouch, R. K., and Menick, D. R. (1999) The proton release group of bacteriorhodopsin controls the rate of the final step of its photocycle at low pH. *Biochemistry 38*, 2026−2039.
(29) Morgan, J. E., Vakkasoglu, A. S., Lanyi, J. K., Lugtenburg, J., Gennis, R. B., and Maeda, A. (2012) Structure changes upon deprotonation of the proton release group in the bacteriorhodopsin photocycle. *Biophys. J. 103*, 444−452.
(30) Garczarek, F., Brown, L. S., Lanyi, J. K., and Gerwert, K. (2005) Proton binding within a membrane protein by a protonated water cluster. *Proc. Natl. Acad. Sci. U.S.A. 102*, 3633−3638.
(31) Garczarek, F., and Gerwert, K. (2006) Functional waters in intraprotein proton transfer monitored by FTIR difference spectroscopy. *Nature 439*, 109−112.
(32) Wolf, S., Freier, E., Potschies, M., Hofmann, E., and Gerwert, K. (2010) Directional proton transfer in membrane proteins achieved through protonated protein-bound water molecules: A proton diode. *Angew. Chem., Int. Ed. 49*, 6889−6893.
(33) Bashford, D., and Gerwert, K. (1992) Electrostatic calculations of the pK_a values of ionizable groups in bacteriorhodopsin. *J. Mol. Biol. 224*, 473−486.
(34) Govindjee, R., Misra, S., Balashov, S. P., Ebrey, T. G., Crouch, R. K., and Menick, D. R. (1996) Arginine-82 regulates the pKa of the group responsible for the light-driven proton release in bacteriorhodopsin. *Biophys. J. 71*, 1011−1023.
(35) Luecke, H., Schobert, B., Richter, H. T., Cartailler, J. P., and Lanyi, J. K. (1999) Structural changes in bacteriorhodopsin during ion transport at 2 angstrom resolution. *Science 286*, 255−261.
(36) Clemens, M., Phatak, P., Cui, Q., Bondar, A. N., and Elstner, M. (2011) Role of Arg82 in the early steps of the bacteriorhodopsin proton-pumping cycle. *J Phys Chem B 115*, 7129−7135.
(37) Luecke, H., Schobert, B., Cartailler, J. P., Richter, H. T., Rosengarth, A., Needleman, R., and Lanyi, J. K. (2000) Coupling photoisomerization of retinal to directional transport in bacteriorhodopsin. *J. Mol. Biol. 300*, 1237−1255.
(38) Száraz, S., Oesterhelt, D., and Ormos, P. (1994) pH-induced structural changes in bacteriorhodopsin studied by Fourier transform infrared spectroscopy. *Biophys. J. 67*, 1706−1712.
(39) Dioumaev, A. K., Brown, L. S., Needleman, R., and Lanyi, J. K. (2001) Coupling of the reisomerization of the retinal, proton uptake, and reprotonation of Asp-96 in the N photointermediate of bacteriorhodopsin. *Biochemistry 40*, 11308−11317.
(40) Zscherp, C., Schlesinger, R., Tittor, J., Oesterhelt, D., and Heberle, J. (1999) In situ determination of transient pK_a changes of internal amino acids of bacteriorhodopsin by using time-resolved attenuated total reflection Fourier-transform infrared spectroscopy. *Proc. Natl. Acad. Sci. U.S.A. 96*, 5498−5503.
(41) Freier, E., Wolf, S., and Gerwert, K. (2011) Proton transfer via a transient linear water-molecule chain in a membrane protein. *Proc. Natl. Acad. Sci. U.S.A. 108*, 11435−11439.
(42) Tittor, J., Paula, S., Subramaniam, S., Heberle, J., Henderson, R., and Oesterhelt, D. (2002) Proton translocation by bacteriorhodopsin in the absence of substantial conformational changes. *J. Mol. Biol. 319*, 555−565.
(43) Subramaniam, S., and Henderson, R. (2000) Molecular mechanism of vectorial proton translocation by bacteriorhodopsin. *Nature 406*, 653−657.
(44) Oesterhelt, D. (1982) Photophosphorylation and reconstitution of photophosphorylation in halobacterial cells, in *Biomembranes Part I: Visual Pigments and Purple Membranes, II* (Packer, L., Ed.) pp 349−355, Academic Press, New York.
(45) Liman, E. R., Tytgat, J., and Hess, P. (1992) Subunit stoichiometry of a mammalian K^+ channel determined by construction of multimeric cDNAs. *Neuron 9*, 861−871.
(46) Lang-Hinrichs, C., Queck, I., Büldt, G., Stahl, U., and Hildebrandt, V. (1994) The archaebacterial membrane protein bacterio-opsin is expressed and N-terminally processed in the yeast *Saccharomyces cerevisiae*. *Mol. Gen. Genet. 244*, 183−188.
(47) Pezeshki, S., Chimerel, C., Bessonov, A. N., Winterhalter, M., and Kleinekathöfer, U. (2009) Understanding ion conductance on a molecular level: An all-atom modeling of the bacterial porin OmpF. *Biophys. J. 97*, 1898−1906.
(48) Wang, T., Zheng, J., Facciotti, M. T., and Duan, Y. (2013) Schiff base switch II precedes the retinal thermal isomerization in the photocycle of bacteriorhodopsin. *PLoS One 8*, e69882-1−e69882-11.
(49) Case, D. A., Cheatham, T. E., Darden, T., Gohlke, H., Luo, R., Merz, K. M., Onufriev, A., Simmerling, C., Wang, B., and Woods, R. J. (2005) The Amber biomolecular simulation programs. *J. Comput. Chem. 26*, 1668−1688.
(50) Wang, T., and Duan, Y. (2007) Chromophore channeling in the G-protein coupled receptor rhodopsin. *J. Am. Chem. Soc. 129*, 6970−6971.
(51) Duan, Y., Wu, C., Chowdhury, S., Lee, M. C., Xiong, G., Zhang, W., Yang, R., Cieplak, P., Luo, R., Lee, T., Caldwell, J., Wang, J., and Kollman, P. (2003) A point-charge force field for molecular mechanics simulations of proteins based on condensed-phase quantum mechanical calculations. *J. Comput. Chem. 24*, 1999−2012.
(52) Yaffe, E., Fishelovitch, D., Wolfson, H. J., Halperin, D., and Nussinov, R. (2008) MolAxis: Efficient and accurate identification of channels in macromolecules. *Proteins 73*, 72−86.
(53) Hartmann, R., and Oesterhelt, D. (1977) Bacteriorhodopsin-mediated photophosphorylation in *Halobacterium halobium*. *Eur. J. Biochem. 77*, 325−335.
(54) Michel, H., and Oesterhelt, D. (1976) Light-induced changes of the pH gradient and the membrane potential in *H. halobium*. *FEBS Lett. 65*, 175−178.
(55) Nagel, G., Kelety, B., Möckel, B., Büldt, G., and Bamberg, E. (1998) Voltage dependence of proton pumping by bacteriorhodopsin is regulated by the voltage-sensitive ratio of M1 to M2. *Biophys. J. 74*, 403−412.
(56) Nagel, G., Möckel, B., Büldt, G., and Bamberg, E. (1995) Functional expression of bacteriorhodopsin in oocytes allows direct measurement of voltage dependence of light induced H+ pumping. *FEBS Lett. 377*, 263−266.
(57) Geibel, S., Friedrich, T., Ormos, P., Wood, P. G., Nagel, G., and Bamberg, E. (2001) The voltage-dependent proton pumping in bacteriorhodopsin is characterized by optoelectric behavior. *Biophys. J. 81*, 2059−2068.
(58) Weber, W. (1999) Ion currents of *Xenopus laevis* oocytes: State of the art. *Biochim. Biophys. Acta 1421*, 213−233.
(59) del Rosario, R. C., Oppawsky, C., Tittor, J., and Oesterhelt, D. (2010) Modeling the membrane potential generation of bacteriorhodopsin. *Math. Biosci. 225*, 68−80.
(60) Geibel, S., Lörinczi, E., Bamberg, E., and Friedrich, T. (2013) Voltage dependence of proton pumping by bacteriorhodopsin mutants with altered lifetime of the M intermediate. *PLoS One 8*, e73338-1−e73338-11.
(61) Mukohata, Y., and Kaji, Y. (1981) Light-induced membrane-potential increase, ATP synthesis, and proton uptake in *Halobacterium halobium*, R1mR catalyzed by halorhodopsin: Effects of N,N′-dicyclohexylcarbodiimide, triphenyltin chloride, and 3,5-di-*tert*-butyl-4-hydroxybenzylidenemalononitrile (SF6847). *Arch. Biochem. Biophys. 206*, 72−76.
(62) Matsuno-Yagi, A., and Mukohata, Y. (1980) ATP synthesis linked to light-dependent proton uptake in a rad mutant strain of *Halobacterium* lacking bacteriorhodopsin. *Arch. Biochem. Biophys. 199*, 297−303.
(63) Matsuno-Yagi, A., and Mukohata, Y. (1977) Two possible roles of bacteriorhodopsin; a comparative study of strains of *Halobacterium*

halobium differing in pigmentation. *Biochem. Biophys. Res. Commun. 78*, 237−243.
(64) Hartmann, R., Sickinger, H. D., and Oesterhelt, D. (1980) Anaerobic growth of halobacteria. *Proc. Natl. Acad. Sci. U.S.A. 77*, 3821−3825.
(65) Avetisyan, A. V., Kaulen, A. D., Skulachev, V. P., and Feniouk, B. A. (1998) Photophosphorylation in alkalophilic halobacterial cells containing halorhodopsin: Chloride-ion cycle? *Biochemistry (Moscow) 63*, 625−628.
(66) Michel, H., and Oesterhelt, D. (1980) Electrochemical proton gradient across the cell membrane of *Halobacterium halobium*: Comparison of the light-induced increase with the increase of intracellular adenosine triphosphate under steady-state illumination. *Biochemistry 19*, 4615−4619.